

Electronic Supplementary Information

Dual-Wavelength Lasing from Organic Dye Encapsulated Metal-Organic Framework Microcrystals†

Yue Zhang,^{‡a} Haiyun Dong,^{‡b} Yuan Liu,^{‡a} Chunhuan Zhang,^b Fengqin Hu,^{*a} and Yong Sheng Zhao^{*b}

^a College of Chemistry, Beijing Normal University, Beijing 100875, China. E-mail: fqhu@bnu.edu.cn

^b Key Laboratory of Photochemistry, Institute of Chemistry, Chinese Academy of Sciences, Beijing 100190, China. E-mail: yszhao@iccas.ac.cn

[‡] Y. Zhang, H. Dong and Y. Liu contributed equally to this work.

Contents

- i. **Experimental details.**
 - 1). Materials.
 - 2). Preparation of dye@MOF composite microcrystals.
 - 3). Characterizations.
- ii. **Fig. S1.** The crystal structure of rho-ZMOF and chemical structure of the two dye molecules.
- iii. **Fig. S2.** Magnified scanning electron microscopy (SEM) image of rho-ZMOF microcrystals.
- iv. **Schemes S1.** Schematic illustration for the formation of the DASPI&LDS 750@rho-ZMOF microcrystals via an ion-exchange process.
- v. **Fig. S3.** X-ray diffraction patterns of rho-ZMOF, DASPI@rho-ZMOF, LDS 750@rho-ZMOF and DASPI&LDS 750@rho-ZMOF.
- vi. **Fig. S4.** Emission spectra of two kinds of pure dye@MOF microcrystals and corresponding dye powders.
- vii. **Fig. S5.** Schematic illustration of home-built far-field microphotoluminescence system.
- viii. **Fig. S6.** Emission spectra and threshold cure of DASPI&LDS 750@rho-ZMOF microcrystals with different $R_{L/D}$ values under increasing pump densities at 532 nm.
- ix. **Fig. S7.** Emission spectra of the DASPI&LDS 750@rho-ZMOF microcrystals with $R_{L/D} = 0.45$ under different pump densities at 532 nm.

Experimental details

Materials: Trans-4-[4-(dimethylamino)styryl]-1-methylpyridinium iodide (DASPI) and 2-[4-[4-(dimethylamino)phenyl]-1,3-butadienyl]-3-ethyl-naphtho[2,1-d]thiazolium perchlorate (LDS 750) were purchased from Sigma-Aldrich and used without further purification. The rho-ZMOF microcrystals were synthesized via a solvothermal reaction of indium nitrate hydrate, 4,5-imidazolecarboxylic acid, and 1,3,4,6,7,8-hexahydro-2H-pyrimido[1,2-a]pyrimidine as described in the literature.¹

Preparation: The dye@rho-ZMOF composite microcrystals (DASPI@rho-ZMOF, LDS 750@rho-ZMOF and DASPI-LDS 750@rho-ZMOF) were prepared through an ion-exchange method: rho-ZMOF crystals were immersed in a solution of dye (DASPI or LDS 750 or mixture of DASPI and LDS 750) in DMF at 60 °C for 3 days. Subsequently, the resulting crystals were filtered off, washed several times with DMF until no characteristic color was observed in the filtrate, and then dried at 60 °C for 4 hours.

Characterization: The morphology and crystallinity of dye@MOF microcrystals were characterized with scanning electron microscopy (SEM, FEI, Nova NanoSEM 450) and X-ray diffraction (XRD, Philips X'pert PRO). The absorption and fluorescence spectra were measured on a UV-visible spectrometer (Shimadzu UV-2600) and a fluorescent spectrometer (Hitachi F-7000), respectively. PL images were taken with an Olympus FluoView-500 inverted microscope. To measure the micro-area PL spectra, the dye@MOF microcrystals were excited locally with a semiconductor laser (532nm). The optically pumped lasing measurements were performed on a home-build far-field microphotoluminescence system (Fig. S4).

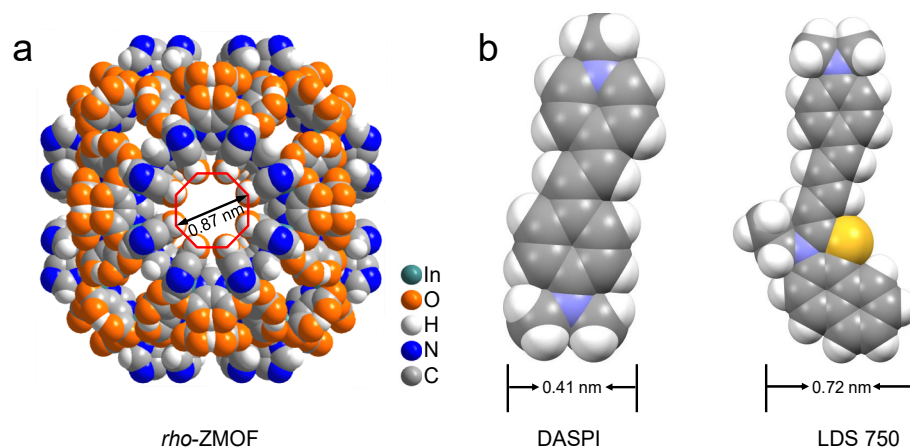


Fig. S1. The crystal structure of *rho*-ZMOF and chemical structure of the two dye molecules.

In the crystal of *rho*-ZMOF, each indium metal ion is coordinated to four nitrogen atoms and four oxygen atoms of four separate HImDC ligands, generating large pores measuring 0.87 nm in diameter. DASPI (lateral dimension of 0.41 nm) and LDS 750 (lateral dimension of 0.72 nm) were chosen as the guest gain material, which is smaller than the pores of the MOF, providing the opportunity for dye molecule to enter the MOF.

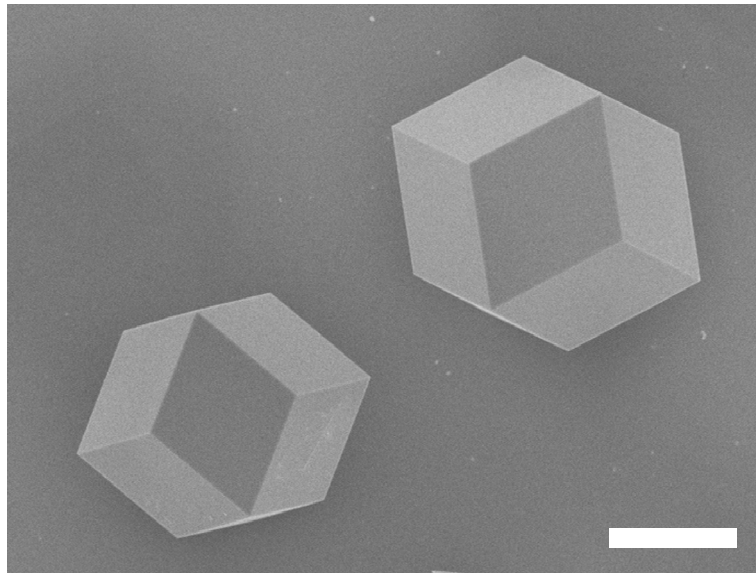
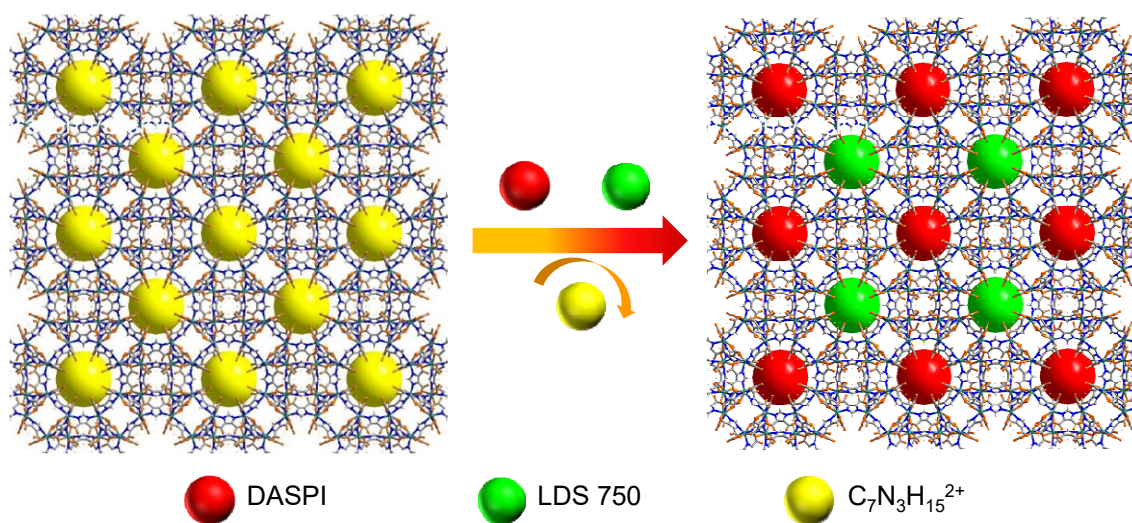


Fig. S2. Magnified SEM image of *rho*-ZMOF microcrystals. Scale bar is 20 μm .

From the magnified SEM image of the *rho*-ZMOF microcrystals, we can see that the as-prepared microcrystals have regularly shaped morphology with smooth surfaces and flat end facets. This would minimize the optical scattering loss and efficiently reflect the guided emission, which is beneficial for the achievement of strong microcavity effects. These outstanding optical properties would make the MOF microcrystal function as high-quality-factor optical microcavity.



Schemes S1. Schematic illustration for the formation of the DASPI&LDS 750@*rho*-ZMOF microcrystals via an ion-exchange process.

The internal pores of *rho*-ZMOF contain a large number of $C_7N_3H_{15}^{2+}$ cations, which allows the introduction of cationic dyes DASPI or LDS 750 via an ion-exchange process. Due to the strong ionic interaction, the guest dyes can be well trapped in the pores of the MOFs.

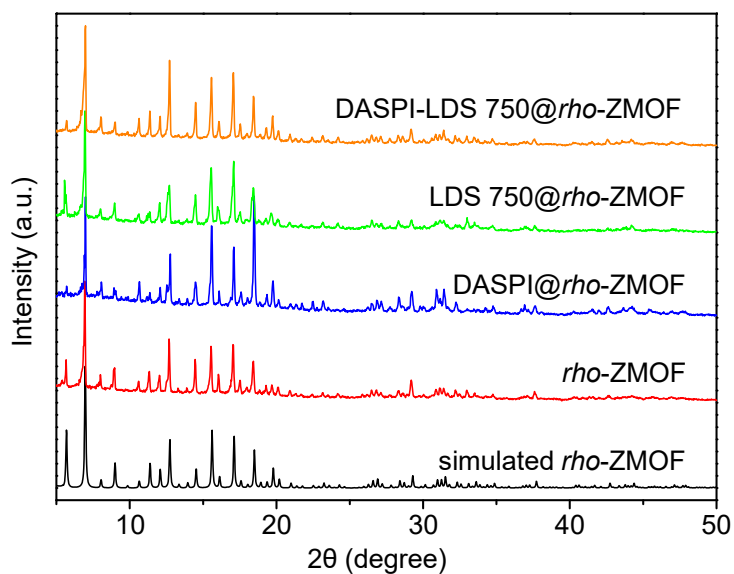


Fig. S3. X-ray diffraction patterns of *rho*-ZMOF, DASPI@*rho*-ZMOF, LDS 750@*rho*-ZMOF and DASPI&LDS 750@*rho*-ZMOF.

As shown in Fig. S3, the X-ray powder diffraction (XRD) patterns of *rho*-ZMOF powder well match those of the simulated results from the single crystal diffraction, clearly indicating that pure *rho*-ZMOF phase was obtained. When DASPI or LDS 750 dyes were encapsulated into *rho*-ZMOF, the patterns remained unchanged, indicating that the intactness of internal porous framework structure during the ion-exchange process for well-matched diffraction peaks between the dye-exchanged MOFs and parent *rho*-ZMOF.

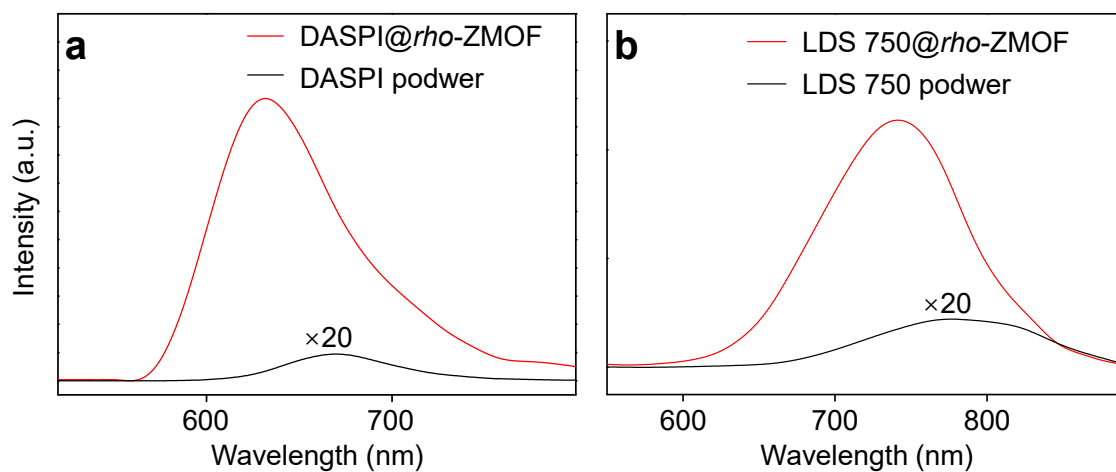


Fig. S4. Emission spectra of two kinds of pure dye@MOF microcrystals and corresponding dye powders

Compared with powders, both DASPI and LDS 750 exhibit enhanced luminescence after being incorporated into *rho*-ZMOF microcrystals. This enhanced luminescence reveals that the dispersion of the dye molecules into the *rho*-ZMOF pores effectively avoid the aggregation-caused quenching effect.

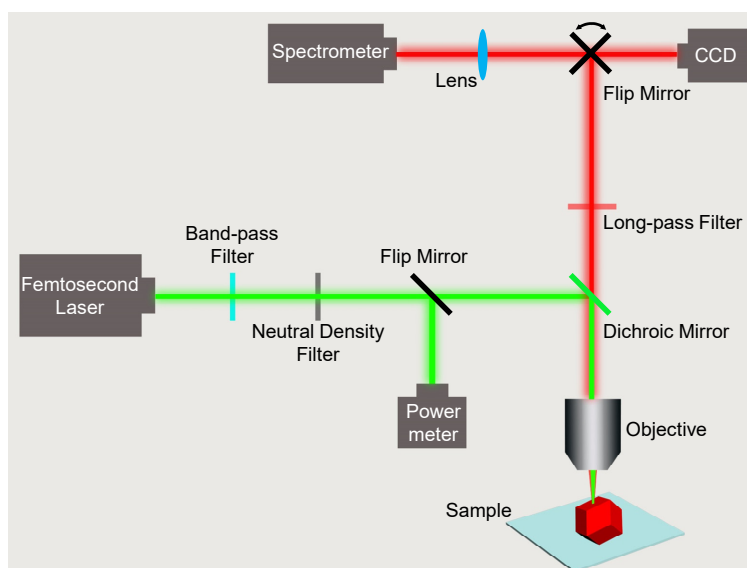


Fig. S5. Schematic illustration for the home-built far-field microphotoluminescence system.

The optically pumped lasing measurements were performed on a home-built far-field microphotoluminescence system. The excitation pulses (470, 532, and 570 nm) were generated from an optical parametric amplifier (Light Conversion TOPAS) that was pumped by a regenerative amplifier (Spectra Physics, 800 nm, 100 fs, 1 kHz), which was in turn seeded by a mode-locked Ti:sapphire laser (Mai Tai, Spectra Physics, 800 nm, 100 fs, 80 MHz). The excitation laser was filtered with a 532 nm band-pass filter and then focused down to a 30 μm diameter spot through an objective lens (Nikon CFLU Plan, 20 \times , N.A. = 0.5). The power at the input was altered by a neutral density filter. The emissions from the individual dye@MOF microcrystals were collected by the same objective with the back-scattering configuration. The emission signals are imaged on a CCD camera and analyzed by the spectrometer after removing the excitation beam with a 590 nm long-pass filter.

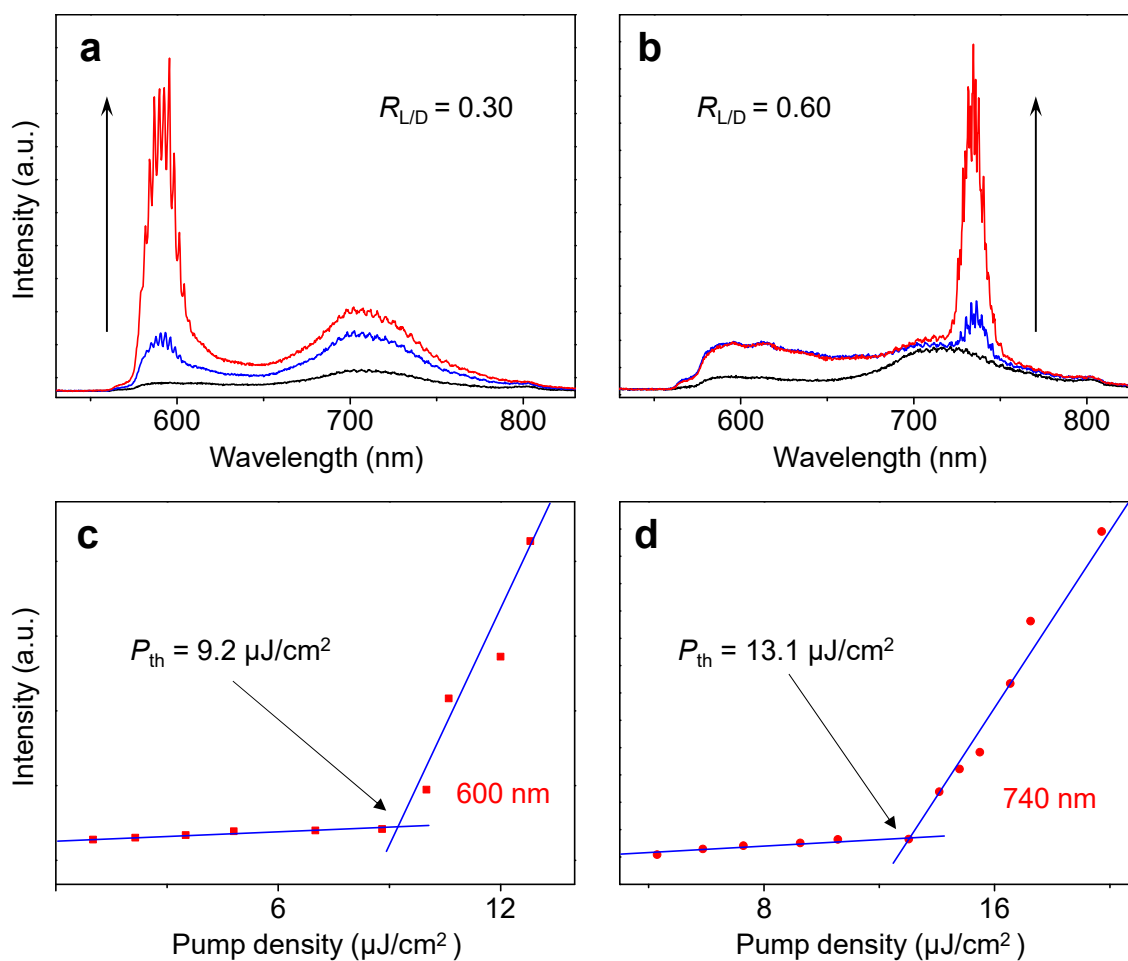


Fig. S6. Emission spectra and threshold cure of DASPI&LDS 750@rho-ZMOF microcrystals with different R_{LD} values under increasing pump densities at 532 nm.

When the LDS 750/DASPI content ratio $R_{LD} = 0.3$ and 0.6 , the lasing actions from DASPI&LDS 750@rho-ZMOF microcrystals occurs at ~ 600 nm and ~ 740 nm, which can be attributed to the stimulated emission of the DASPI and LDS 750 molecules, respectively.

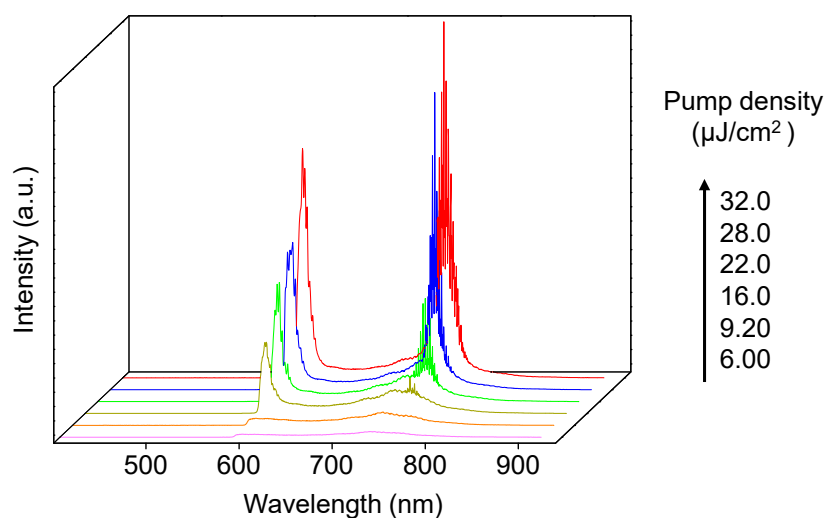


Fig. S7. Emission spectra of the DASPI&LDS 750@rho-ZMOF microcrystals with $R_{L/D} = 0.45$ under different pump densities at 532 nm.

As shown in Fig. S7, the DASPI&LDS 750@rho-ZMOF microcrystals sustain stable dual-wavelength lasing output in a wide pump density range. No mutual interference between the two lasing bands was observed even at high pump densities ($P > 2P_{th}$). Such stable dual-wavelength lasing property can be attributed to the spatial confinement effect of the MOF pores that suppresses the intermolecular interaction between different organic dyes.

1. Y. Liu, H. Dong, K. Wang, Z. Gao, C. Zhang, X. Liu, Y. S. Zhao and F. Hu, *ACS Appl. Mater. Interfaces*, 2018, **10**, 35455-35461.